Cardiac CT Platforms: State of the Art

6

Bernhard Schmidt, Katharine Grant, Thomas G. Flohr, and Thomas Allmendinger

Shorter scan times and the desire for higher resolution were the driving forces behind the development of spiral scanning in 1990 and the first multi-detector row computed tomography (CT) systems in 1998 [1–6]. With the introduction of ECG-gated scanning on four-slice CT scanners in 1999, the first step toward cardiac imaging with multi-detector row computed tomography (MDCT) had been made.

Available since 2004, 64-slice CT systems are currently considered prerequisite for routine cardiac imaging in clinical scenarios [7–10], and with its introduction, the task of imaging coronary arteries and calcium scoring replaced EBCT (electron beam CT) completely. 64-slice CT scanners allowed for comprehensive diagnosis of morphology and cardiac function within one integrated CT examination, including high-resolution imaging of the coronary arteries [11–14]. Improved temporal resolution (< 200 ms) was enabled by faster gantry rotation times down to 0.33 s and leading to an increased clinical robustness of ECG-gated scanning techniques at higher heart rates [9, 10]. ECG-gated 64-slice CT also started being used for rapid triage of patients with acute chest pain in the emergency room and for diagnosis of pulmonary embolism, aortic dissection or aneurysm, or significant coronary artery disease in one scan.

Despite the new clinical opportunities and the increasing use of CT for routine cardiac imaging, several challenges still remained: For high heart rates, multi-segment reconstructions allowing for temporal resolutions beyond half the rotation time were still desired for robust imaging of coronary arteries. Multi-segment reconstructions unfortunately do not guarantee images with a well-defined improved temporal resolution in combination with the need for redundant data and thus due to acquisitions with reduced pitch resulting in substantially increased patient dose values [15]. Irregular or arrhythmic heart rates posed a challenge for artifact-free combination of images that were reconstructed from multiple cardiac cycles into a single volume, often yielding "stack artifacts" in these cases. Moreover, calcium blooming was still an issue – mainly due to operation in an X-ray tube limited, and therefore noise-dominated regime, resulting in the routine application of medium-sharp reconstructions in cardiac images exhibiting the undesired blooming of high-contrast calcium. Adaption of X-ray tube voltages (kVs) to lower kVs to reduce patient dose was used in particular for regular contrast-enhanced scans, to improve image quality in pediatric patients. These adaptations occurred manually, often on weight-based selection criteria, and application was limited to a select group of the general population due to the demand of high X-ray tube current capacities required for cardiac imaging [16]. Finally, scan times for coronary CTAs were still in the range of 10–15 s given the limited detector coverage and the lack of alternative scan technology.

In 2004, all major CT vendors offered 64-slice CT scanners. The remaining challenges of cardiac CT imaging, the pursuit for even more clinical applications, the risk that MR imaging could further improve on and replace CT for not just functional but for morphological imaging, the tenacious competition of the vendors, and the relentless improvements in engineering and scientific innovations, made cardiac imaging the main driving force for further CT innovations, technical developments, and new CT platforms. In contrary to previous innovations, technical solutions and directions of development differed substantially between different vendors, ranging from wide detector systems with single-source systems over two X-ray source systems with a single detector to systems with two X-ray tubes and two detectors.

In 2005, a dual-source CT (DSCT) system, i.e., a CT system with two X-ray tubes and two corresponding detectors offset by 90°, was introduced [17]. It provided improved

B. Schmidt (✉) · T. Allmendinger · T. G. Flohr
Department of Computed Tomography, Siemens Healthcare GmbH, Forchheim, Germany
e-mail: bernhard.schmidt@siemens.com

K. Grant
Siemens Medical Solutions USA, Inc., Malvern, PA, USA

U. J. Schoepf (ed.), *CT of the Heart*, Contemporary Medical Imaging, https://doi.org/10.1007/978-1-60327-237-7_6

temporal resolution of 83 ms independent of the patient's heart rate as compared to 165–190 ms with MDCT systems at that time. DSCT scanners proved to be well suited for integrated cardiothoracic examinations even in acutely ill patients and for the triage of patients with acute chest pain [18]. The introduction of dual-energy scanning with DSCT enabled tissue characterization and provided combined functional and morphological information, i.e., to depict local perfusion deficits in the lung parenchyma in patients with pulmonary embolism [19, 20].

The second and third generations (introduced in 2009 and 2013, respectively) of DSCT systems offer high-pitch scan modes which enabled coverage of the heart in a single cardiac cycle [21, 22]. In addition, high-resolution CT scans of the entire thorax in less than 1 s scan time with an acquisition time per image better than 100 ms were now possible [23, 24]. These scan modes are potentially advantageous for evaluating the lung parenchyma and vascular structures in patients who have difficulty complying with breath-holding instructions [25]. High-pitch scan modes have also been used for fast CTA scans of the aorta [26]. Combined with ECG triggering, they provide adequate visualization of the coronary arteries, the aortic valve, the aorta, and the iliac arteries in one scan at low radiation dose, which is beneficial in the planning of transcatheter aortic valve replacement (TAVR) procedures [27, 28].

Another challenge for CT is the visualization of dynamic processes in extended anatomical ranges, i.e., to characterize the inflow and outflow of contrast agent in the arterial and venous system in dynamic CT angiographies or to determine the enhancement characteristics of the contrast agent in volume perfusion studies. One way to address this problem is by utilizing wide-area detectors large enough to cover organs such as the heart, the kidneys, or the brain in one axial scan. Besides temporal resolution, registration or mismatch artifacts from the combination of multiple cardiac cycles or slabs in z-direction are another challenge, naturally leading to the idea of increasing the detector coverage to such a level that the entire heart is covered in a single prospectively gated sequential acquisition. Meanwhile, two vendors have introduced CT scanners with 16 cm detector coverage at isocenter, providing 320×0.5 mm collimation at 0.28 s rotation time or 256×0.625 mm collimation at 0.28 s rotation time [29]. Additionally these scanners have the potential to acquire dynamic volume data by repeatedly scanning the same anatomical range without table movement (e.g., [30–32]).

In the following sections, after a short historic review of EBCT, general technical demands of MDCT for cardiac image quality are discussed. Then a technical overview of the main currently available platforms and CT systems is provided, and details about advantages and technical challenges of the different approaches are discussed.

From EBCT to Multi-detector CT for Cardiac Imaging

EBCT

Generation of X-rays for medical imaging is typically accomplished by using X-ray tubes. Electrons emitted from a cathode are accelerated by a high-voltage power source and collide with the anode, at which X-rays are generated by the interaction of electrons within the anode material. For CT imaging, X-ray attenuation data from multiple angles around the patient are required. Thus, first CT systems were equipped with X-ray tubes set up opposite a detector, which in conjunction rotated around the patients at rotation times of about 5 s or longer. Mechanical constraints and challenges with rotating components, mainly data and power transmission, prevented continuous rotation at faster rotation times back then. Unfortunately, for cardiac imaging in particular, faster rotation times were desired to minimize motion artifacts and provide better temporal resolution. Already in the late 1970s, electron beam scanners were proposed with the goal of providing a substantially higher temporal resolution for cardiac imaging by avoiding rotating parts. In the early 1980s, D.P. Boyd – a Stanford researcher and partner in the radiology department at the University of California, San Francisco (USA) – invented the first clinically used EBCT system: "Electron beam control assembly and method for a scanning electron beam computed tomography scanner." It related to "… a high speed multiple section computed-tomographic (CT) x-ray transmission scanner and more particularly to a multiple target scanning-electron beam x-ray source providing rapid scan …" (see also Figs. 6.1 and 6.2) [33]. Instead of rotating tube and detector around the patient, a stationary detector ring is used for data acquisition. To generate X-rays, an electron beam originating from an electron gun is deflected and steered over an anode that was ringlike enclosing the patient. Temporal resolutions of 100 ms and shorter were possible. The main application – in particular in the early days of EBCT – was the detection and quantification of coronary calcium at dose levels of about 0.6 mSv [34]. Later on, studies reported the use of EBCT for coronary CTA imaging [35], assessment of ventricular anatomy and function [36], as well as myocardial perfusion [37].

Despite the unquestionable benefit of high temporal resolution of EBCT, only a few systems were installed worldwide, by the end of 1987 about 14 units. The high price, low production volume, system design issues (e.g., the inability to use scatter collimators), and limited clinical benefit beside the heart were preventing cardiologists and radiologists to invest into an EBCT system. Finally, the limited spatial resolution was yet another factor making the already niche scanner even less attractive. Although with the latest generation of EBCTs (GE's e-Speed), slice thicknesses of 1.5 mm were

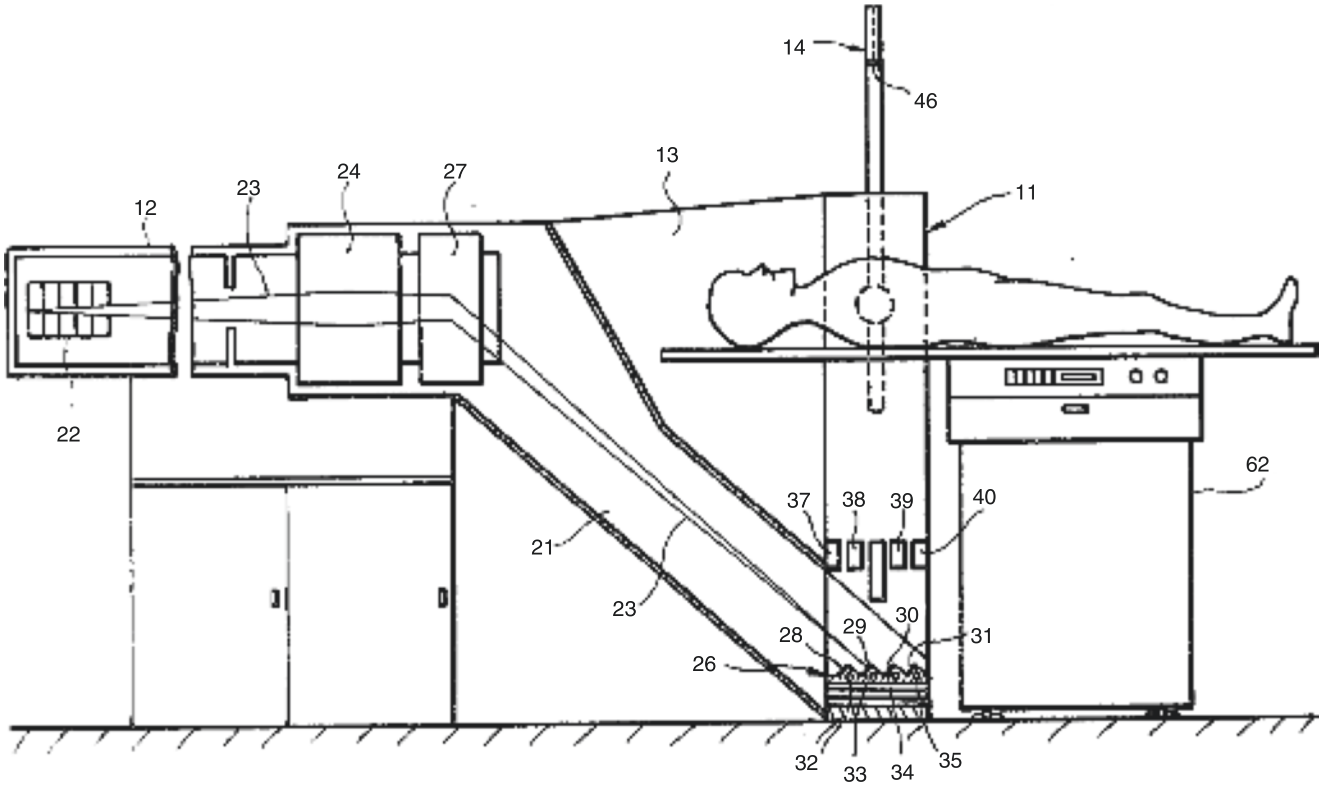

Fig. 6.1 Illustration of an EBCT (electron beam computerized tomography) system – taken from Boyd's patent in 1982; US 4352021: Electrons emitted from the electron gun [22] are accelerated and steered around the patient. The electron beam hitting the target rings [28–31] created X-rays at the respective position on the ring. From there the X-rays passed through the patient to the detector [14] on the opposite end of the scan tube tomography system. (From US patent US4352021 https://www.google.com/patents/US4352021?dq=us+patent+4352021&hl=en&sa=X&ved=0ahUKEwitp6_N38vYAhXDY98KHT01DXwQ6AEIJzAA)

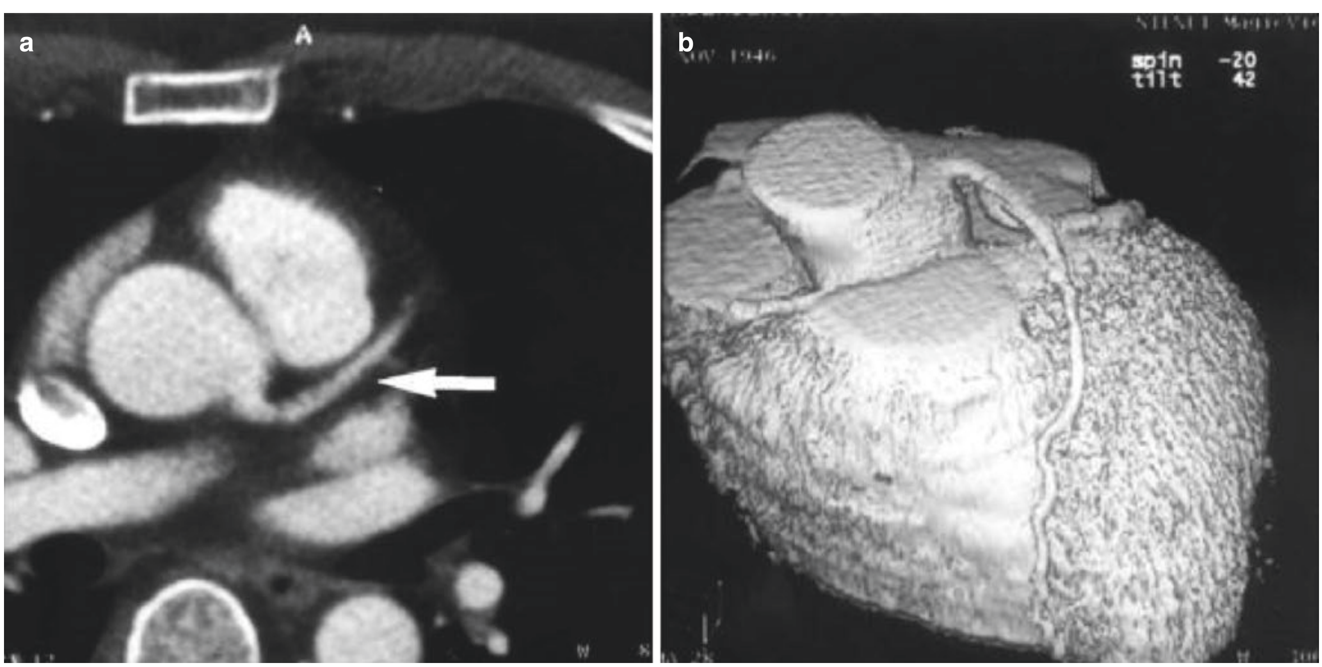

Fig. 6.2 Axial image of a contrast-enhanced EBCT scan, showing the left main and left anterior descending coronary artery (arrow) (**a**). Surface-rendered view of the heart by visualizing only voxels above a certain threshold (**b**) (From Achenbach et al. [35], with permission)

enabled [38], this relevant specification parameter for coronary CT imaging was already matched by 16-slice CT systems at the end of 1990s and then outperformed substantially by the introduction of 64-slice MDCT systems providing routinely submillimeter image resolution in the early 2000s. In addition, volume scanning, the ability to apply modern dose reduction techniques such as low kV scanning, utilization of shaped filters, or patient-specific tube current modulation never became available or were technically impossible to implement on an EBCT system.

Multi-detector Row CT Setup (MDCT)

The basic CT system design of modern MDCT system is shown in Fig. 6.3. Today, all manufacturers use the same fan-beam CT design, characterized by an X-ray tube and an opposing detector which are mounted on a rotating gantry ring. The detector is a two-dimensional array, consisting of 2–320 element rows aligned in the *z*-axis direction (the *z*-axis is the length axis of the patient) and around 650–1000 detector elements in each row. The fan angle of the detector is wide enough (approximately 45–55°) to cover a whole-body scan field of view (SFOV) of typically 50 cm in diameter. In a CT scan, the detector array measures the X-ray attenuation profile of the patient at 1000–5000 different angular positions depending on the rotation time, during a full gantry rotation. All measurement values acquired at the same angular position of the measurement system are called a "projection" or "view." Slip ring designs which pass the electrical signals across sliding contacts allow for continuous rotation of the measurement system.

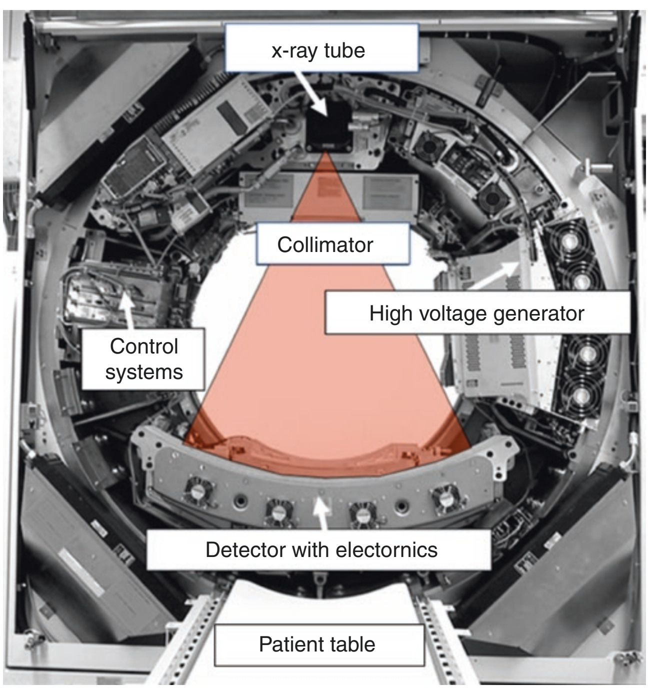

Fig. 6.3 Main components of a modern MDCT system. The X-ray fan beam is indicated in red; it covers a SFOV of typically 50 cm in diameter. The data measurement system consists of detector and detector electronics. The patient is positioned within the gantry using a dedicated patient table

State-of-the-art X-ray tubes are powered by onboard generators and provide peak powers of 60–120 kW at different user-selectable voltages ranging from 70 to 150 kV. Scanning at low tube voltage is favorable for dose-efficient scans, such as pediatric CT [39, 40] or CT angiographic scanning [16, 41–43], because the X-ray attenuation of iodine significantly increases at lower kV [40].

All modern MDCT systems use solid-state scintillation detectors. The incident X-rays interact with a radiation-sensitive crystal or ceramic (such as gadolinium oxide, gadolinium oxysulfide, or garnets) with suitable doping. They are absorbed, and their energy is converted into visible light which is detected by a silicon photodiode attached to the backside of the scintillation detector. The resulting electrical current is then converted into a digital signal. Key requirements for a detector material are good detection efficiency, i.e., high atomic number, very good signal linearity, and very short afterglow time to enable fast readout at the high gantry rotation speeds that are essential for cardiothoracic CT.

The image noise in a CT image is caused by the quantum noise of the X-ray photons and the electronic noise of the detection system. In high-dose scanning situations, the image noise is dominated by quantum noise, whereas when larger patients are scanned or in examinations at low radiation dose, e.g., in low-dose thorax scans, electronic noise is more dominant. In addition, electronic noise degrades image quality and the stability of CT values. Recently, detector systems with integrated electronics were commercially introduced (e.g., Stellar, Siemens Healthcare, Forchheim, Germany; NanoPanel Elite, Philips Healthcare, Amsterdam, Netherlands), with the goal of reducing electronic noise and detector cross talk. In these designs, photodiodes and analog-to-digital converters (ADC) are combined and directly attached to the ceramic scintillators, without the need for noise-sensitive analog connection cables (Fig. 6.4). In a recent study, for a 30 cm phantom corresponding to an average abdomen, reduction of image noise by up to 40% was demonstrated with the use of an integrated electronic detector at 80 kV [44]. According to the authors, this noise reduction translated into a dose reduction of up to 50% while achieving equivalent image noise.

In early MDCT detectors, ADC electronics and data transmission were a limiting factor and a strong contributor to the total cost of a system. An efficient way of enabling higher scan speeds based on a larger *z*-axis collimation was through the development of detector elements with a larger number of detector rows. The total beam width in the *z*-

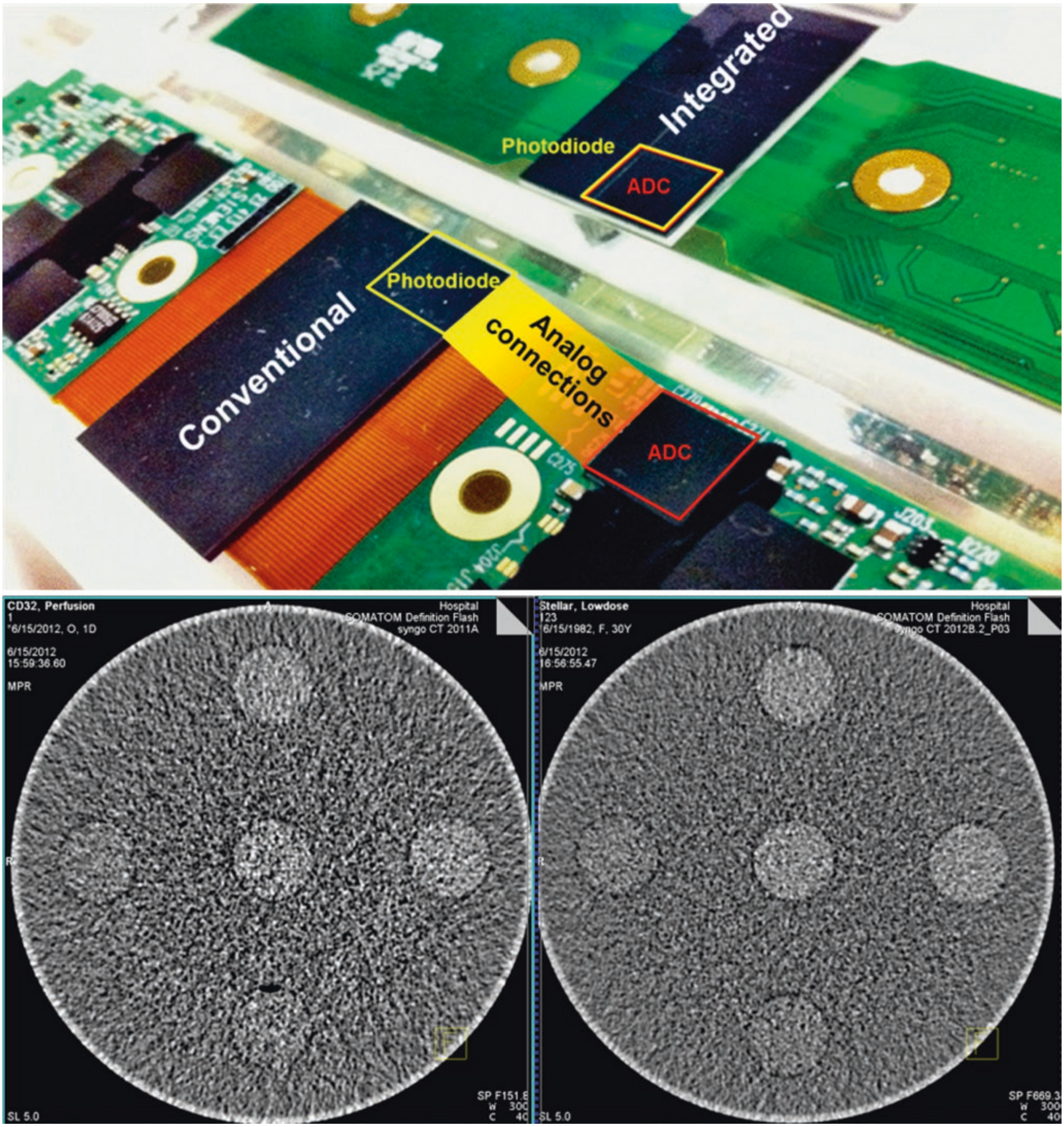

Fig. 6.4 Comparison of the Si-tile without scintillator ceramics – with and without integrated electronics (top) (Siemens Healthcare). At the bottom CT images of a 30 cm water phantom acquired at same dose (80 kV, 30 mA) are illustrated. The integrated design leads to substantially lower noise values (right bottom image)

direction is subsequently adjusted by pre-patient collimation at the expense of fusing two (or more) detectors along the *z*-axis electronically into thicker slices.

The detector of a 16-slice CT (Siemens SOMATOM Emotion 16) as an example comprises 16 central rows, each with 0.6 mm collimated slice width, and 4 outer rows on either side, each with 1.2 mm collimated slice width – in total, 24 rows with a *z*-width of 19.2 mm at isocenter (Fig. 6.5). By adjusting the X-ray beam width such that only the central detector rows are illuminated, the system provides 16 collimated 0.6 mm slices. By illuminating the entire detector, reading out all rows and electronically combining the signals of every 2 central rows, the system provides 16 collimated 1.2 mm slices. The 16-slice detectors of other

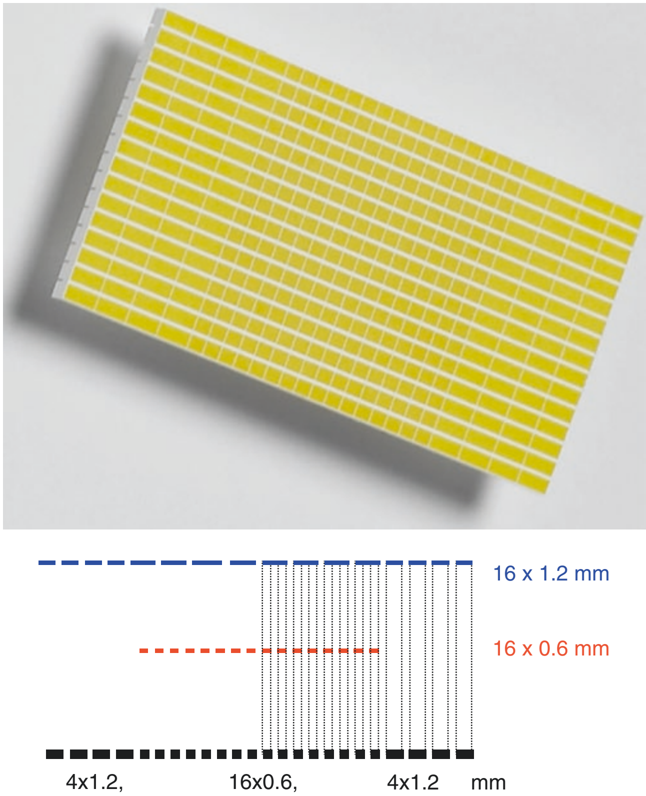

Fig. 6.5 Example of a 16-slice detector, which consists of 24 detector rows and provides either 16 collimated 0.6 mm slices or – by combination of the signals of every 2 central rows – 16 collimated 1.2 mm slices

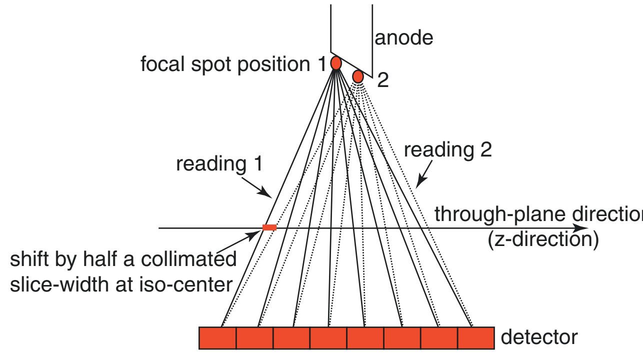

Fig. 6.6 Basic principle of a *z*-flying focal spot. Consecutive readings are shifted periodically by half a slice width on the anode plate. Every two readings are interleaved to one projection with double the number of slices and half the *z*-sampling distance

manufacturers are similarly designed, with slightly different collimated slice widths (0.5 mm, 0.6 mm, or 0.625 mm, depending on the manufacturer).

With the introduction of MDCT detectors with 64 or more detector rows and a vendor-dependent minimal slice width of 0.5 mm, 0.6 mm, or 0.625 mm, the detector row fusing mechanisms described above was no longer necessary. As of today a wide variety of detector row configurations exist (e.g., 96 × 0.6 mm, *z*-width 6 cm at the isocenter; 128 × 0.625 mm, *z*-width 8 cm at the isocenter) up to the widest commercially available CT detectors covering 16 cm at isocenter. The acquisition is either based on 320 collimated 0.5 mm slices (Aquilion ONE, Toshiba Medical, Japan) or 256 collimated 0.625 mm slices (Revolution, GE Healthcare, USA).

All modern MDCT scanners enable reconstruction of images with different image slice widths from the same raw data according to the clinical needs (e.g., 3 mm or 5 mm for initial viewing and additional submillimeter slices or 1 mm slices for post processing).

Some CT systems employ a hardware-based oversampling scheme effectively doubling the number of simultaneously acquired slices by means of a *z*-flying focal spot [45, 46] (Z-FFS, Siemens Healthcare, Forchheim, Germany; Ingenuity DAS, Philips Healthcare, Amsterdam, Netherlands). The focal spot in the X-ray tube is periodically moved between two *z*-positions on the anode plate by electromagnetic deflection. As a consequence, the measurement rays of two readings are shifted by half a collimated slice width at isocenter and can be interleaved to one projection with double the number of slices but half the *z*-sampling distance (Fig. 6.6). Two 64-slice readings with 0.6 mm slice width and 0.6 mm *z*-sampling distance, as an example, are combined to one projection with 128 overlapping 0.6 mm slices at 0.3 mm *z*-sampling distance. The *z*-flying focal spot provides improved data sampling in the *z*-direction for better through-plane resolution, reconstruction of thinner slices, and reduced spiral windmill artifacts (Fig. 6.7).

ECG-Based Imaging with MDCT

To acquire images of the heart, recording of the ECG signal is mandatory. On one hand one wants to be able to process and view a dedicated phase of the cardiac cycle which requires a time stamp-based link between the cardiac phase of the patient and the acquired CT data. On the other hand, in the case of limited detector coverage, data from multiple heart beats is acquired over time and then stitched together to allow the reconstruction and display of the whole heart. For MDCT with 64 or more detector rows, typically two different acquisition modes are used – ECG-gated spiral/helical and prospective ECG-triggered sequence acquisition. More details about data acquisition and reconstruction are provided in Chaps. 6 and 11. However, to illuminate recent technical developments in CT technology, a short summary of the acquisition techniques and influencing parameters on coverage and temporal resolution is provided.

During the first years of routine clinical integration of coronary CT angiography, retrospectively ECG-gated spiral (helical) scanning was the most widely used data acquisition

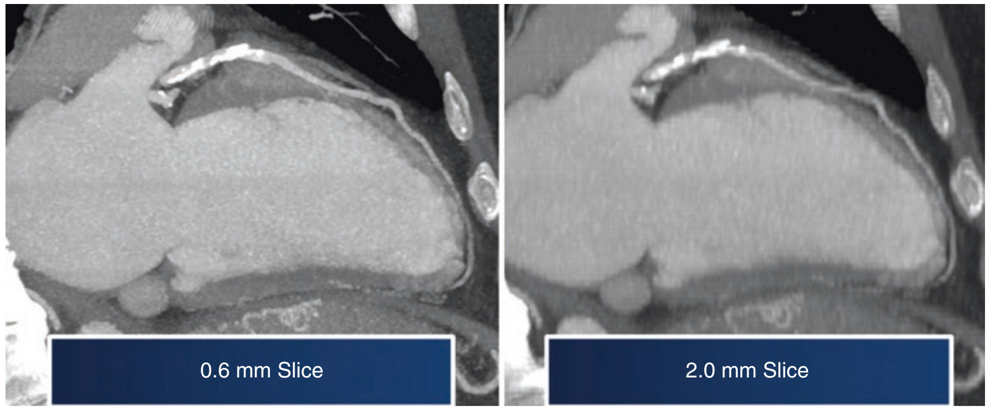

Fig. 6.7 Impact of slice thickness on resolution. *Z*-flying focal spot techniques allow for the reconstruction of thinner slices and this sharper delineation of anatomical structures

technique. A spiral CT scan with continuous data acquisition and table movement at low table feed (low spiral pitch of approximately 0.2) is performed to examine the patient's heart. Simultaneously, the patient's ECG is recorded. Following data acquisition, the ECG serves as guidance to select those data intervals in the spiral CT data set that describe the same user-selected cardiac phase, measured in different cardiac cycles. Those data are then used for phase-consistent image reconstruction of the coronary anatomy. The upper part of Fig. 6.8 shows the principle of retrospectively ECG-gated spiral scanning. This scan mode is very versatile because it allows for retrospective optimization of the reconstruction window and image reconstruction in different cardiac phases.

As a downside, retrospectively ECG-gated spiral scanning of the heart requires strongly overlapping spiral data acquisition at low table feed for phase-consistent imaging and is therefore associated with relatively high radiation dose to the patient, which can be somewhat reduced by using ECG-controlled dose modulation approaches ("ECG-pulsing"). Many modern CT scanners are equipped with such versatile ECG-pulsing algorithms which react flexibly to arrhythmia and ectopic beats and have the potential to extend the clinical application spectrum of ECG-synchronized dose modulation to patients with irregular heart rates.

As an alternative scan mode, prospectively ECG-triggered sequential scanning in a "step-and-shoot" technique is more commonly used with newer generations of CT systems. During the CT examination, the patient's ECG is used to trigger the start time for the acquisition of axial (sequential) CT images; see lower part of Fig. 6.8. The patient table is moved to its defined start position: with a user-selectable temporal distance from an R-wave, an axial CT scan without table movement is performed. The CT system acquires scan data covering a sub-volume of the patient's cardiac anatomy which corresponds to around 90% of the total *z*-width for a 64-row detector and is reduced for CT systems with large detectors in the *z*-axis direction which have to cope more with cone-beam effects. The table is then moved to the next *z*-position, and the next axial CT scan is performed at the corresponding temporal distance from the next R-wave. This way, the heart volume is sequentially covered by axial scans.

ECG-triggered axial scanning is a very dose-efficient scan technique. In a simple technical realization, a partial scan data interval – the minimum amount of data necessary for image reconstruction – is acquired in a user-selected phase of the patient's cardiac cycle. Then, however, neither retrospective reconstruction in a slightly different phase of the patient's cardiac cycle to minimize motion artifacts is possible nor are multiphase reconstructions for evaluation of cardiac function. Furthermore, due to the fact that incomplete data is acquired, the temporal offset of scan data acquisition to the next R-wave is based on a prospective estimate of the previous cycle's length. This is a challenge in patients with irregular heart beat and arrhythmia, unless the acquisition strategy is properly tailored and aimed at an end-systolic cardiac phase [47].

From 4 cm MDCT CT Systems to Area Detector and Dual-Source CT

Area Detector CT

ECG-synchronized CT volume imaging of the heart acquired by the abovementioned MDCT systems typically results in 3–4 sub-volumes reconstructed from data measured over multiple consecutive heart beats (Fig. 6.9) [48]. Variations of heart motion from one cardiac cycle to the next, as well as contrast media dynamics between the cycles, can result in these image sub-volumes being shifted relative to each other and, as a consequence, resulting in stairstep or slab registration artifacts in multi-planar reformations (MPRs) or volume rendered images (VRTs). Recently, 128-row, 256-slice CT systems with 80 mm *z*-axis coverage were commercially introduced (Philips ICT, Philips Healthcare, Best, the Netherlands). They facil-

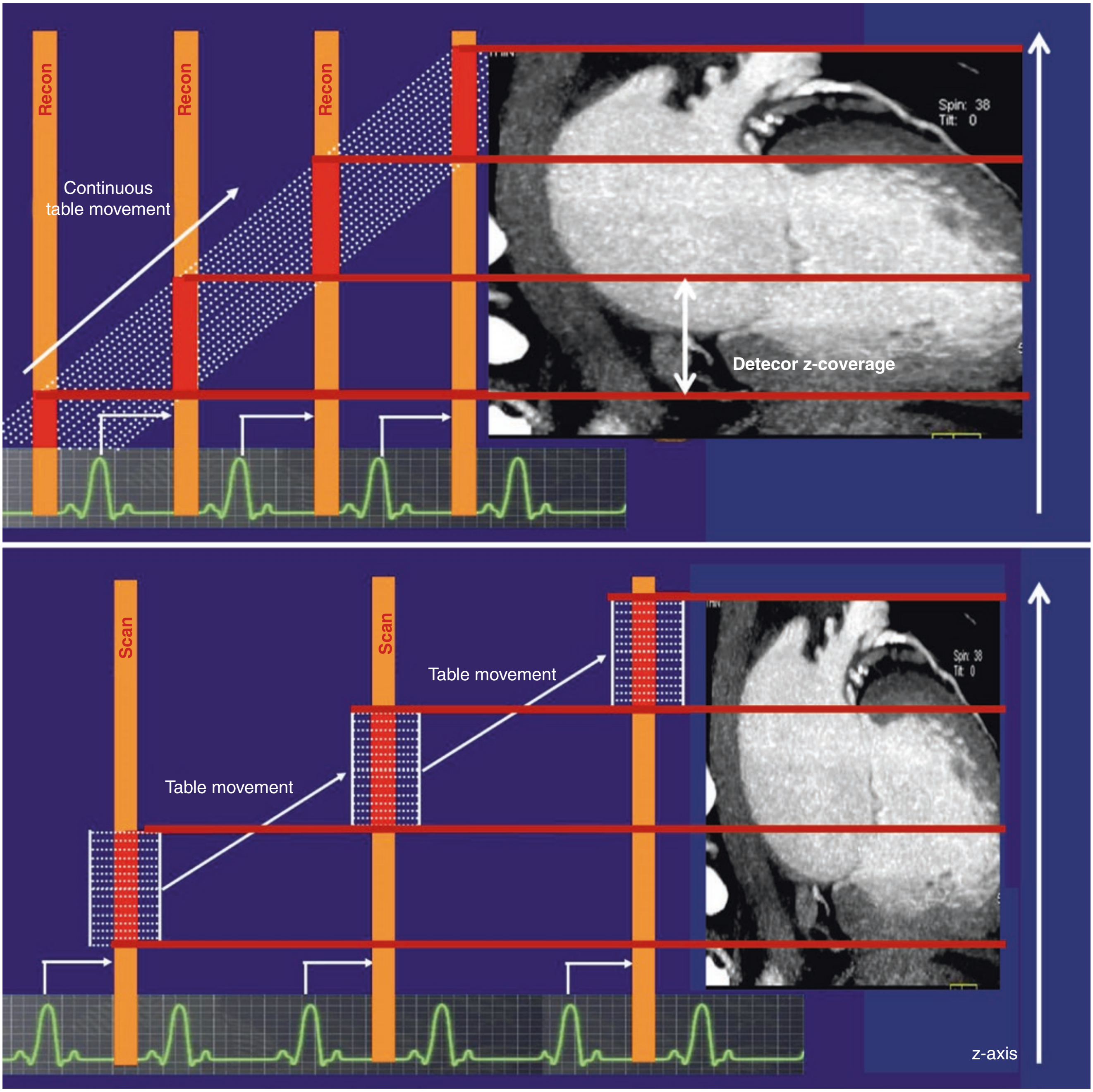

Fig. 6.8 Established acquisition modes for cardiac scanning with CT systems up to 4 cm coverage: In retrospective ECG-gated scan mode (upper part), a helical scan with a comparatively small, fixed heart rate-dependent table feed is performed. For higher heart rates, table feed is increased. In case of a 4 cm system, after 3–4 heart beats, the heart is covered. Similar scan times are accomplished in prospectively ECG-triggered axial (sequential) scanning of the heart (lower part). Based on the user-selected phase position of ECG signal, an axial scan is performed. After each axial scan, the table moves to the next *z*-position. This acquisition technique is also called "step-and-shoot"

itate examinations of the heart with two axial scans, thereby reducing the number of potential "steps" in the volume image to one [49]. In a study with 160 consecutive patients, prospectively triggered axial coronary CTA performed on 256-slice CT provided significantly improved and more stable image quality at an equivalent effective radiation dose compared with 64-slice CT [50].

As of today, two CT vendors provide single-source CT systems with large area detectors capable of imaging the entire heart in one beat, using one axial scan without table movement. With 320 × 0.5 mm collimation at 0.28 s rotation time (Toshiba Aquilion ONE, Toshiba Medical Systems Corporation, Tokyo, Japan) and 256 × 0.625 mm collimation at 0.28 s rotation time (GE Revolution, GE Healthcare, Waukesha, USA), these systems can cover 16 cm in the *z*-axis direction at isocenter, large enough to cover the entire heart in one beat and hence avoid stairstep and slab registration artifacts, as well as problems related to inconsistent contrast enhancement in different sub-volumes [51].

A possible consequence of the large cone-beam angle that those systems have compared to systems with smaller *z*-coverage can be limitations in the field of view available for reconstruction (Fig. 6.10). In addition, due to this effect also dose efficiency is compromised since not all acquired data can be utilized fully for the reconstruction of the images. Another challenge of larger detector *z*-coverage is increased X-ray scatter. Scattered radiation may cause hypo-dense cupping or streaking artifacts, and the scatter-induced noise may reduce the contrast-to-noise ratio (CNR) in the images [52]. To reduce scatter – in this case forward scatter – some vendors have added scatter grids. While anti-scatter grids are a well-known topic for dual-source CT systems, it is important to note that anti-scatter grids are also recommended in the case of single-source system with wide detectors. A study by Engel et al. showed that the contribution of scatter for a 16 cm single-source system is even higher than in the case of an 8 cm dual-source system, which again motivates the need for anti-scatter grids (ASG) even for single-source systems in case of wide detectors [53]. The requirements were intensely evaluated by Vogtmeier et al. [54]. Figure 6.11 shows the impact on scatter for 1D and 2D scatter grids, for different collimations. In particular, for collimations between 8 and 16 cm coverage, the 2D grids performed substantially better.

Another challenge of area detectors are the often necessary changes to the tube design. In order to compensate for the so-called Heel effect and to accomplish a homogeneous intensity on the detector along the scan direction (Fig. 6.12), the anode angle is often flatted [55]. The intensity profile is improved, however, at the price of reduced tube power. This consequence can also be seen when looking at the maximum

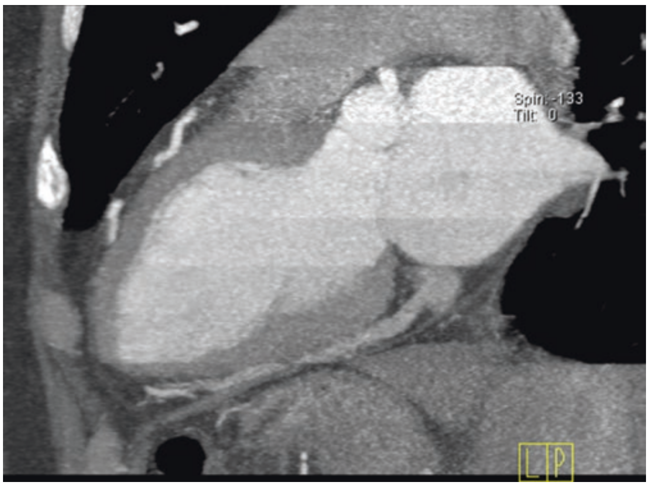

Fig. 6.9 Non-axial view of a cardiac examination performed with ECG-gated spiral mode. Due to the limited coverage, slab artifacts are pronounced due to contrast dynamics and a slight phase mismatch between different acquired heart beats combined with limited temporal resolution

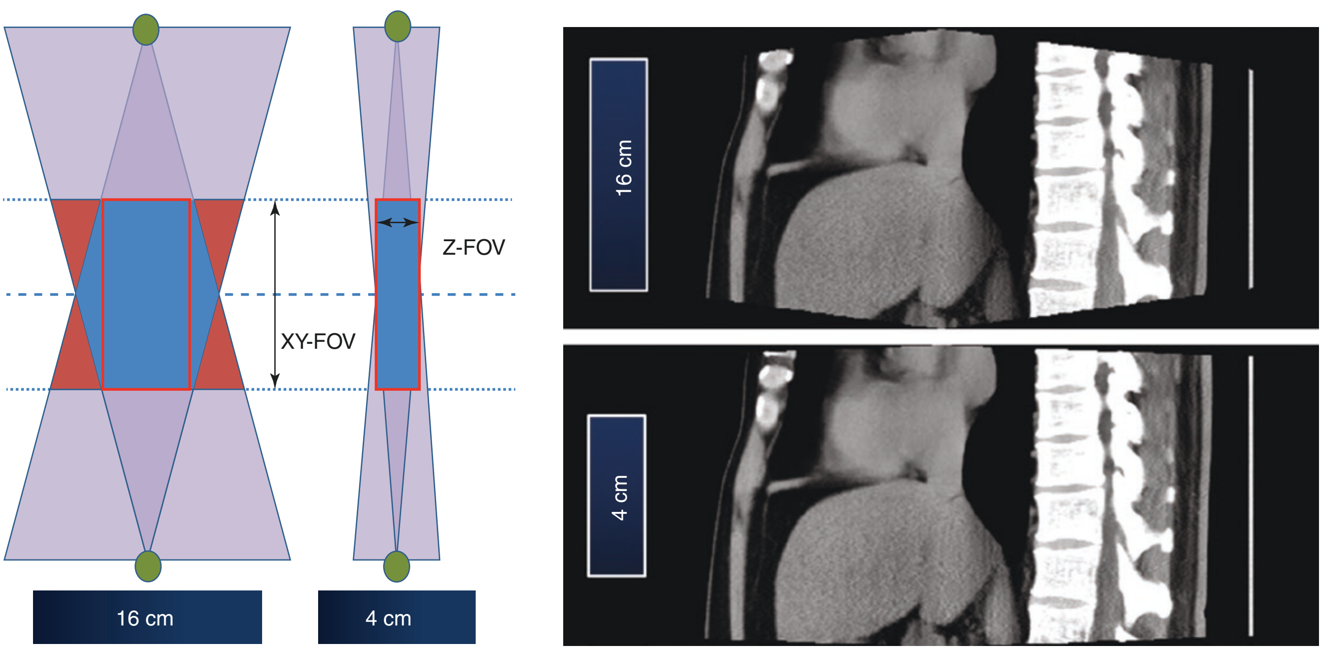

Fig. 6.10 Comparison of systems with 16 cm and 4 cm detector coverage in axial scan mode. Left side: view from the side. The area of full FOV is substantially reduced in case of wide detector systems. Although regions are exposed (highlighted in red), they cannot be reconstructed with traditional reconstruction techniques. As a consequence distorted regions are often cropped in the reconstructed images (see right side)

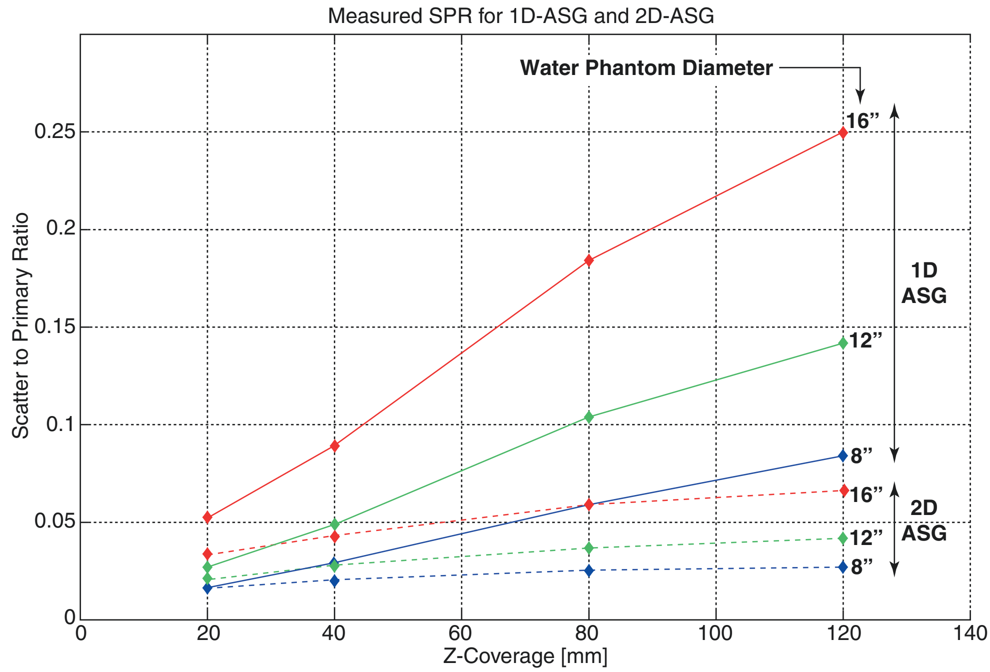

Fig. 6.11 Contribution of scatter to the primary signal for different collimations and designs of anti-scatter grid (ASG). (From Engel et al. [53], with permission)

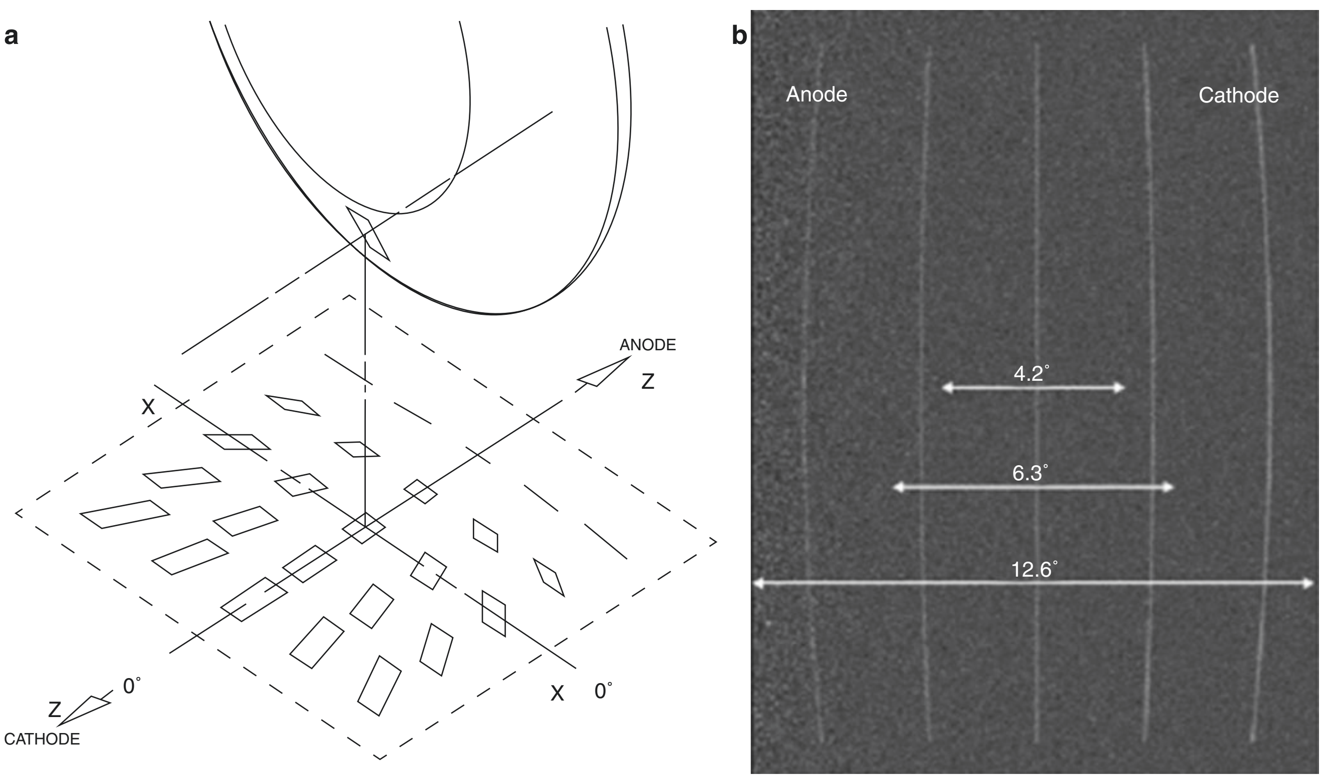

Fig. 6.12 Due to the Heel effect, the footprint of the projected focal spot becomes much narrower on the anode side. To compensate and have a more homogeneous intensity, typically the anode angle is changed to a flatter design. The drawback might be a reduced power output of the tube. (From Li et al. [55], with permission)

tube currently available on high-end CTs. For non-16 cm systems, tube currents up to 1000 mA (Philips) and 1300 mA (Siemens) are enabled, whereas the 16 cm systems have maximum mA values of 735 mA (GE) and 600 mA (Toshiba).

Despite all the abovementioned challenges, successful use of CT systems with 16 cm detector coverage for coronary CTA has been demonstrated [53, 56, 57]. The application spectrum has been extended to scanning of patients with atrial fibrillation [58] and coronary CTA combined with first pass perfusion evaluation [59, 60]. The second generation of 320-row CT scanners has been shown to enable coronary CTA at reduced radiation dose compared to the first generation [52, 56].

As a second benefit, CT systems with wide-area detectors can acquire dynamic volume data by repeatedly scanning the same anatomical range without table movement. This is useful in dynamic CT angiographic examinations or for whole heart functional data acquisition. So et al. published first results on phantoms and an animal model, demonstrating general feasibility for the quantitative evaluation of the myocardial blood flow [61].

As discussed above in detail, systems with 16 cm detectors suffer multiple limitations. Some of the challenges are related to the X-ray source. To compensate for some of the effects, multiple sources in z-direction have been proposed (Fig. 6.13). Fast alternating switching is realized between two X-ray tubes during data acquisition. Due to the improved geometry setup, this approach does not suffer, for example, from cone-beam artifacts compared to traditional wide-area 16 cm CT systems. A commercially available system of this kind was introduced in 2016 (SpotLight CT, Arineta Ltd., Israel). Optimized for a small footprint, the system has a diagnostic field of view limited to 250 mm, 192 detector rows with z-coverage of 140 mm and a fast gantry rotation time of 0.24 s [62]. One can derive from these specifications that the system comprises a highly specialized cardiac CT system in contrast to the above-described multipurpose full-body scanners.

Dual-Source CT

A dual-source CT (DSCT) is a CT system with two X-ray tubes and two detectors at an angle of approximately 90° (Fig. 6.14). Both measurement systems acquire CT scan data simultaneously at the same anatomical level of the patient (same z-position).

The first generation of DSCT scanners with 2 × 64 slices using z-flying focal spot (19.2 mm detector coverage) and 0.33 s gantry rotation time was introduced in 2006 (SOMATOM Definition, Siemens Healthcare, Forchheim, Germany), the second generation with 2 × 128 slices

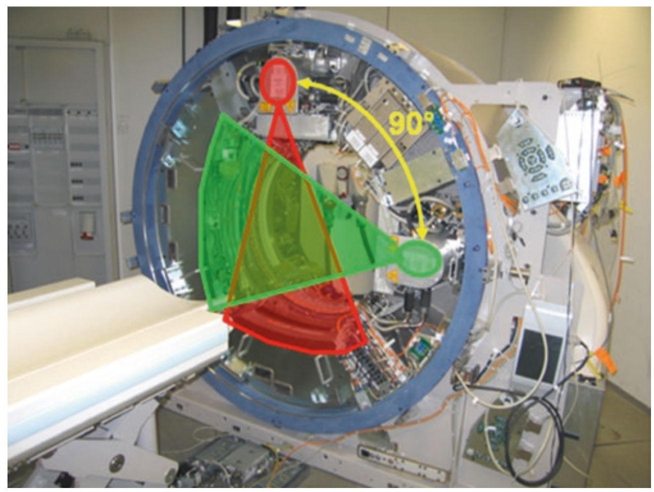

Fig. 6.14 DSCT with two independent measurement systems. The image shows the first-generation DSCT with an angle of 90° between both measurement systems. To increase the SFOV of detector B, an angle of 95° was chosen for the second- and third-generation systems

Fig. 6.13 Setup of CT system in so-called inverse geometry

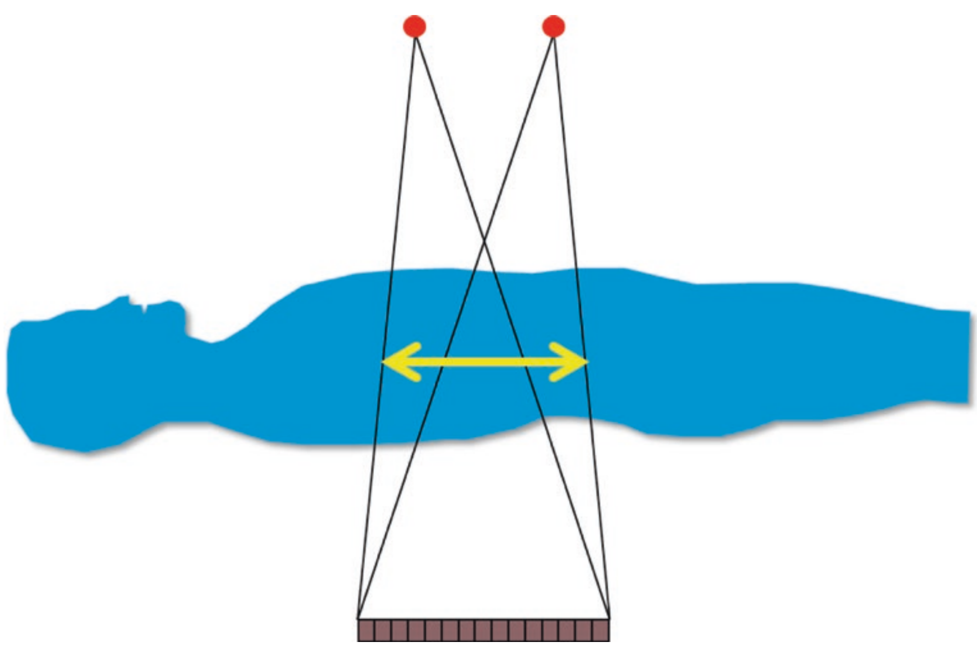

(38.4 mm detector coverage) and 0.28 s gantry rotation time in 2009 (SOMATOM Definition Flash, Siemens Healthcare, Forchheim, Germany), and the third generation with 2 × 192 slices (57.6 mm detector coverage) and 0.25 s gantry rotation time in 2014 (SOMATOM Definition Force, Siemens Healthcare, Forchheim, Germany).

DSCT systems provide significantly improved temporal resolution for cardiothoracic imaging. The shortest data acquisition time for an image corresponds to a quarter of the gantry rotation time. Close to the isocenter, 180° of scan data is the minimum needed for image reconstruction. Due to the 90° angle between both X-ray tubes, each of the measurement systems needs to acquire only 90° of scan data. The two 90° segments at the same anatomical level are put together to form the 180° scan. Using this technique, a temporal resolution of 83 ms, 75 ms, and 66 ms, respectively, is achieved for the three generations of DSCT systems. With the dual-source approach, temporal resolution is independent of the patient's heart rate, because data from only one cardiac cycle are used to reconstruct an image. This is a major difference to single-source MDCT systems, which can provide similar temporal resolution by combining data from several heart cycles to an image in a multi-segment reconstruction. Then, however, temporal resolution strongly depends on the relation of heart rate and gantry rotation time. Meanwhile, several clinical studies have demonstrated the potential of DSCT to reliably perform coronary CT angiographic studies in patients with high and even irregular heart rates (e.g., [63–65]). DSCT is sufficiently accurate to diagnose clinically significant coronary artery disease in difficult to image patients [66, 67]. The high temporal resolution is also beneficial for reducing motion artifacts in cardiothoracic studies (e.g., [68]).

With a DSCT system, both X-ray tubes can also be operated at different kV settings, e.g., 80 and 140 kV, to acquire dual-energy CT data. The advantages and disadvantages of different techniques to acquire dual-energy CT data as well as clinically relevant applications will be discussed substantially more in detail in Chap. 4.

While the maximum spiral pitch in single-source CT images is limited to about 1.5 to ensure gapless volume coverage, DSCT systems can be operated at twice the pitch. Data acquired with the second measurement system a quarter rotation after the first measurement system can be used to fill the sampling gaps up to a pitch of about 3.2 in a limited SFOV that is covered by both detectors [69, 70]. At maximum pitch, no redundant data are acquired, and a quarter rotation of data per measurement system is used for image reconstruction. Temporal resolution is then a quarter of the gantry rotation time. At decreasing pitch, temporal resolution decreases because of the increasing angular data segment that corresponds to an image. At a pitch of 2, for example, temporal resolution is about 0.4 times the rotation time – this is 100 ms with the second-generation DSCT [70].

With the high-pitch scan mode, very high scan speed is achieved – up to 450 mm/s with the second-generation DSCT (38.4 mm detector coverage, 0.28 s gantry rotation time) and up to 737 mm/s with the third-generation DSCT (57.6 mm detector coverage, 0.25 s gantry rotation time). This is beneficial for the examination of larger anatomical ranges in very short scan times, e.g., for chest CTA at high temporal resolution [24], for the evaluation of pulmonary embolism and visualization of most cardiac structures and proximal coronary arteries [71], for fast CTA scans of the aorta at low radiation and contrast dose [72], or when the patient has limited ability to cooperate, such as in pediatric radiology [73–76].

The high-pitch scan mode can also be used in combination with ECG-triggering – the patient's ECG triggers both table motion and data acquisition. The patient table is positioned, and table acceleration is started in a way that the table arrives at the prescribed start z-position (e.g., the base or the apex of the heart) at the requested cardiac phase after full table speed has been reached (Fig. 6.15). Then data acquisition begins. The scan data for images at adjacent z-positions are acquired at slightly different – typically diastolic – phases of the cardiac cycle. Meanwhile, several clinical studies have demonstrated the successful use of the high-pitch scan technique for coronary CT angiography in patients with sufficiently low and stable heart rate (<62 bpm with the second-generation DSCT, <70 bpm with the third-generation DSCT), with the potential to scan the entire heart in one beat at very low radiation dose [23, 77–80].

ECG-triggered high-pitch scans can be used also for comprehensive thorax examinations in the emergency room and in the planning of TAVR procedures, because they provide adequate visualization of the coronary arteries, the aorta, and the iliac arteries in one scan at low radiation dose and high temporal resolution. The very short total scan time may potentially allow for a reduction of the amount of contrast agent; see, e.g., [27, 81]. Figure 6.15 shows an ECG-triggered high-pitch CTA of the aorta as an example.

Despite their clinical benefits, DSCT systems have to cope with some challenges. One challenge is the presence of cross-scattered radiation, i.e., scattered radiation from X-ray tube B detected by detector A and vice versa. Cross-scattered radiation – if not corrected for – can result in image artifacts and degraded CNR of the images [69]. Another challenge is the limited SFOV of the second detector, which was increased from 25 cm in the first-generation DSCT to 35.5 cm in the third-generation DSCT.

The most straightforward correction approach is to directly measure the cross-scattered radiation in detectors A and B and to subtract it from the measured signal. This technique was first implemented in the second-generation

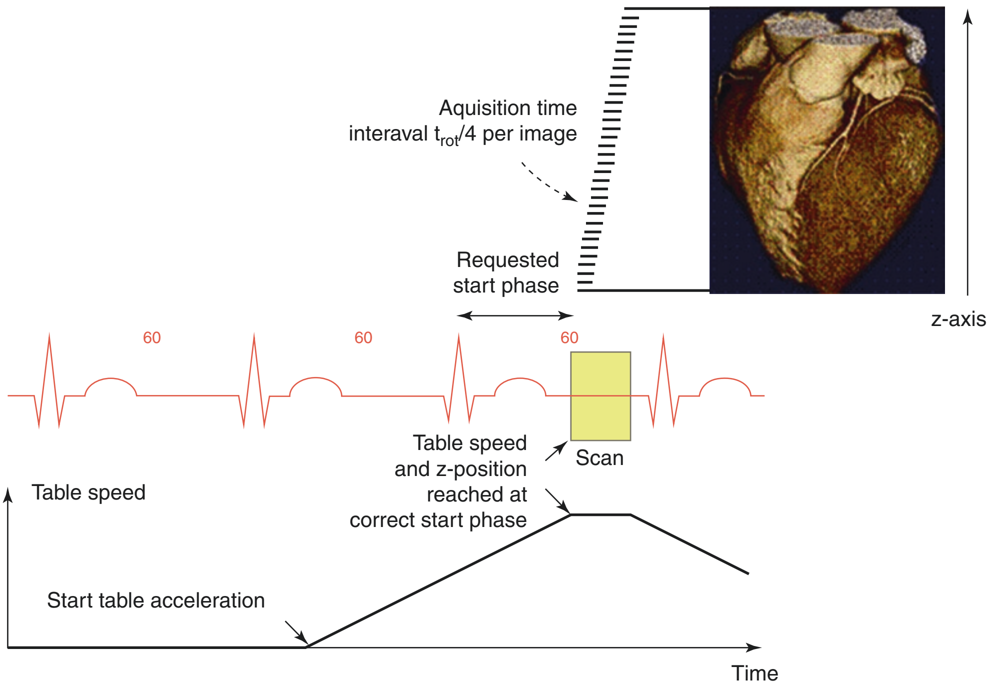

Fig. 6.15 ECG-triggered start of table movement and data acquisition for the high-pitch DSCT spiral

Fig. 6.16 Schematic diagram of a detector module with scatter sensors outside the direct beam. The center region consists of the primary detector pixels, positioned below the collimator blades of the anti-scatter collimator. The scattered radiation sensors, placed on both sides of the primary detector module, are equipped with collimator blades as well. The arrows indicate the *z*-direction (row direction) and the fan-angle direction (channel direction)

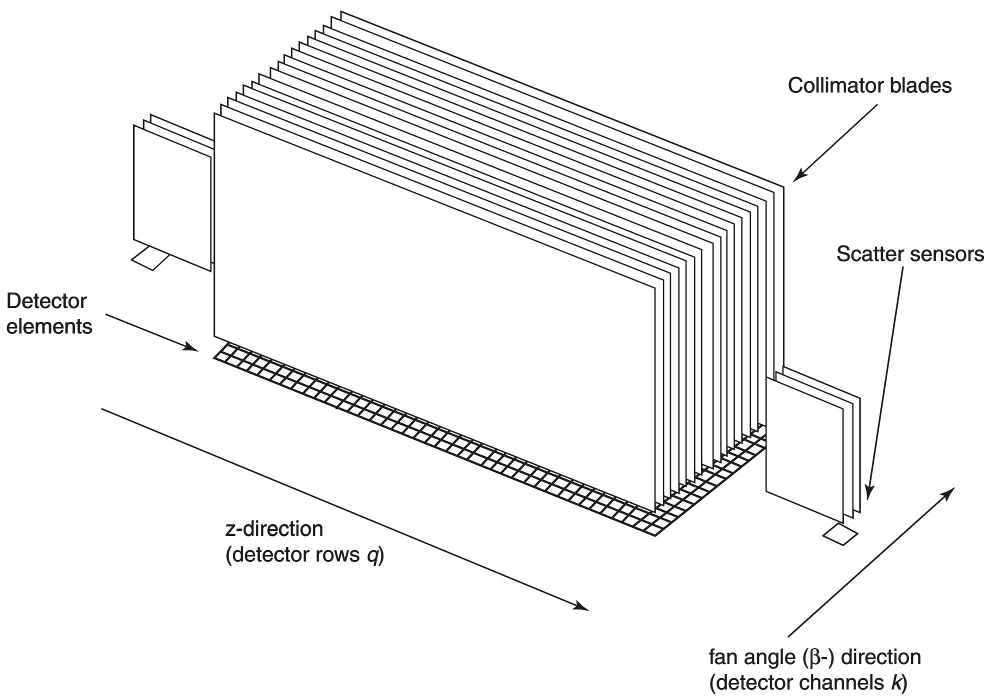

DSCT. It requires additional detector elements on each detector outside the direct beam (Fig. 6.16). An alternative to direct measurement is a model-based cross-scatter correction. The primary source of cross-scattered radiation is Compton scatter at the object surface. In the first-generation DSCT, pre-stored cross-scatter tables for objects with similar surface shape are used for an online correction of the cross-scattered radiation in each measured projection. In the third-generation DSCT, an iterative cross-scatter correction based on a simplified Monte Carlo simulation is applied.

While image artifacts caused by cross-scattered radiation can be significantly reduced by either model-based or measurement-based correction approaches, these corrections are often considered to come at the expense of increased image noise and reduced contrast-to-noise ratio (CNR) in the images. It has been demonstrated, however, that careful low pass filtering of the scatter correction term can efficiently mitigate the image noise increase without visually affecting image detail resolution or image contrast. CNR can in fact be increased beyond the values achieved without cross-scatter correction, and it approaches or sometimes even surpasses the CNR performance of a comparable single-source scan using these techniques.

Another – evitable – challenge of dual-source dual-energy CT (DE) is the 90° offset of projections acquired by both X-ray tubes at the same *z*-position. Because high-energy and low-energy projections are not simultaneously acquired at the same projection angle, raw data-based DE algorithms are difficult to realize. DE algorithms are therefore image based – which has the huge advantage of avoiding the limited and sensitive calibration of raw data-based methods. It is often claimed that image-based methods are strongly limited by the problem of beam hardening. However, under certain conditions – which are typically fulfilled in modern CT scanners – image-based methods are practically equivalent for clinical tasks. A prerequisite for image-based material decomposition is the validity of the thin absorber model. For example, if one uses water and iodine as the basis materials for image-based dual-energy decomposition, the maximum X-ray attenuation of the iodine along any measured ray path is expected to be so small that it is valid to assume a linear contribution to the total attenuation. In clinical practice, this prerequisite is typically fulfilled. If necessary, still dedicated established single energy-based methods for beam-hardening corrections can be applied to allow for respective data correction. As a second prerequisite, both the CT value of water and the CT values of small iodine samples are expected to be independent from their position within the scanned object. DSCT scanners are therefore equipped with an optimized bowtie filter of sufficient beam hardening, and the approximately cylindrical patient cross-section has to be centered within the SFOV – typically being fulfilled in case of clinical CT systems. Anyhow, in practice, electronic noise, scanner calibration, stability of emitted spectra, cone-beam effects, and scattered radiation can have a larger impact on the obtained results than the raw data or image-based analysis method itself. Further on, the ability for an optimized, independent selection of X-ray voltage and spectral filtration – but still dose-wise well and optimally balanced high and low energy beam – and therefore an optimal spectral separation enables robust dual-energy imaging at a huge variety for applications and thus compensates for potential limitations and challenges. Further details are provided in Chap. 4, dedicated to dual-energy imaging of the heart.

A third challenge is the fact that moving objects, such as the heart, are seen by both detectors with an angular offset of about 90°. Motion artifacts in the corresponding A and B images can therefore be slightly different, which can affect the material decomposition of the dual-energy images. In practice, however, this problem is not relevant thanks to the good temporal resolution of DSCT, and it can be further mitigated by nonrigid registration of A and B images.

References

1. Kalender WA, Seissler W, Klotz E, Vock P. Spiral volumetric CT with single-breath-hold technique, continuous transport, and continuous scanner rotation. Radiology. 1990;176(1):181–3.
2. Achenbach S, Ulzheimer S, Baum U, et al. Noninvasive coronary angiography by retrospectively ECG-gated multi-slice spiral CT. Circulation. 2000;102:2823–8.
3. Becker C, Knez A, Ohnesorge B, Schöpf U, Reiser M. Imaging of non calcified coronary plaques using helical CT with retrospective EKG gating. AJR. 2000;175:423–4.
4. Knez A, Becker C, Leber A, Ohnesorge B, Reiser M, Haberl R. Non-invasive assessment of coronary artery stenoses with multidetector helical computed tomography. Circulation. 2000;101:e221–2.
5. Ohnesorge B, Flohr T, Becker C, Kopp A, Schoepf U, Baum U, Knez A, Klingenbeck Regn K, Reiser M. Cardiac imaging by means of electro- cardiographically gated multisection spiral CT – initial experience. Radiology. 2000;217:564–71.
6. Nieman K, Oudkerk M, Rensing B, van Oijen P, Munne A, van Geuns R, de Feyter P. Coronary angiography with multi-slice computed tomography. Lancet. 2001;357:599–603.
7. Hoffmann MHK, Shi H, Schmitz BL, Schmid FT, Lieberknecht M, Schulze R, Ludwig B, Kroschel U, Jahnke N, Haerer W, Brambs H-J, Aschoff AJ. Noninvasive coronary angiography with multislice computed tomography. JAMA. 2005;293:2471–8.
8. Leschka S, Wildermuth S, Boehm T, Desbiolles L, Husmann L, Plass A, Koepfli P, Schepis T, Marincek B, Kaufmann PA, Alkadhi H. Noninvasive coronary angiography with 64-section CT: effect of average heart rate and heart rate variability on image quality. Radiology. 2006;241(2):378–85.
9. Leber AW, Knez A, Ziegler F, Becker A, Nikolaou K, Paul S, Wintersperger B, Reiser MF, Becker CR, Steinbeck G, Boekstegers P. Quantification of obstructive and nonobstructive coronary lesions by 64-slice computed tomography – a comparative study with quantitative coronary angiography and intravascular ultrasound. J Am Coll Cardiol. 2005;46(1):147–54.
10. Raff GL, Gallagher MJ, O'Neill WW, Goldstein JA. Diagnostic accuracy of non-invasive coronary angiography using 64-slice spiral computed tomography. J Am Coll Cardiol. 2005;46(3):552.
11. Salem R, Remy-Jardin M, Delhaye D, Khalil C, Teisseire A, Delannoy-Deken V, Duhamel A, Remy J. Integrated cardio-thoracic imaging with ECG-gated 64-slice multidetector-row CT: initial findings in 133 patients. Eur Radiol. 2006;16(9):1973–81.
12. Bruzzi JF, Rémy-Jardin M, Delhaye D, Teisseire A, Khalil C, Rémy J. When, why, and how to examine the heart during thoracic CT: part 1, basic principles. AJR Am J Roentgenol. 2006;186(2):324–32.
13. Bruzzi JF, Rémy-Jardin M, Delhaye D, Teisseire A, Khalil C, Rémy J. When, why, and how to examine the heart during thoracic CT: part 2, clinical applications. AJR Am J Roentgenol. 2006;186(2):333–41.
14. Delhaye D, Remy-Jardin M, Salem R, Teisseire A, Khalil C, Delannoy-Deken V, Duhamel A, Remy J. Coronary imaging quality in routine ECG-gated multidetector CT examinations of the entire

thorax: preliminary experience with a 64-slice CT system in 133 patients. Eur Radiol. 2007;17(4):902–10.
15. Flohr T, Ohnesorge B. Heart rate adaptive optimization of spatial and temporal resolution for electrocardiogram-gated multislice spiral CT of the heart. J Comput Assist Tomogr. 2001;25(6):907–23.
16. Hausleiter J, Martinoff S, Hadamitzky M, et al. Image quality and radiation exposure with a low tube voltage protocol for coronary CT angiography: results of the PROTECTION II trial. JACC Cardiovasc Imaging. 2010;3(11):1113–23.
17. Flohr TG, McCollough CH, Bruder H, Petersilka M, Gruber K, Süß C, Grasruck M, Stierstorfer K, Krauss B, Raupach R, Primak AN, Küttner A, Achenbach S, Becker C, Kopp A, Ohnesorge BM. First performance evaluation of a dual-source CT (DSCT) system. Eur Radiol. 2006;16(2):256–68.
18. Johnson TR, Nikolaou K, Busch S, Leber AW, Becker A, Wintersperger BJ, Rist C, Knez A, Reiser MF, Becker CR. Diagnostic accuracy of dual-source computed tomography in the diagnosis of coronary artery disease. Investig Radiol. 2007;42(10):684–91.
19. Pontana F, Faivre JB, Remy-Jardin M, Flohr T, Schmidt B, Tacelli N, Pansini V, Remy J. Lung perfusion with dual-energy multidetector-row CT (MDCT): feasibility for the evaluation of acute pulmonary embolism in 117 consecutive patients. Acad Radiol. 2008;15(12):1494–504.
20. Thieme SF, Becker CR, Hacker M, Nikolaou K, Reiser MF, Johnson TR. Dual energy CT for the assessment of lung perfusion--correlation to scintigraphy. Eur J Radiol. 2008;68(3):369–74.
21. Achenbach S, Marwan M, Ropers D, et al. Coronary computed tomography angiography with a consistent dose below 1 mSv using prospectively electrocardiogram-triggered high-pitch spiral acquisition. Eur Heart J. 2010;31(3):340–6.
22. Alkadhi H, Stolzmann P, Desbiolles L, Baumueller S, Goetti R, Plass A, Scheffel H, Feuchtner G, Falk V, Marincek B, Leschka S. Low-dose, 128-slice, dual-source CT coronary angiography: accuracy and radiation dose of the high-pitch and the step-and-shoot mode. Heart. 2010;96(12):933–8. https://doi.org/10.1136/hrt.2009.189100.
23. Lell M, Hinkmann F, Anders K, Deak P, Kalender WA, Uder M, Achenbach S. High-pitch electrocardiogram-triggered computed tomography of the chest: initial results. Investig Radiol. 2009;44(11):728–33.
24. Tacelli N, Remy-Jardin M, Flohr T, Faivre JB, Delannoy V, Duhamel A, Remy J. Dual-source chest CT angiography with high temporal resolution and high pitch modes: evaluation of image quality in 140 patients. Eur Radiol. 2010;20(5):1188–96.
25. Schulz B, Jacobi V, Beeres M, Bodelle B, Gruber T, Lee C, Bauer R, Kerl M, Vogl T, Zangos S. Quantitative analysis of motion artifacts in high-pitch dual-source computed tomography of the thorax. J Thorac Imaging. 2012;27(6):382–6.
26. Beeres M, Schell B, Mastragelopoulos A, Herrmann E, Kerl JM, Gruber-Rouh T, Lee C, Siebenhandl P, Bodelle B, Zangos S, Vogl TJ, Jacobi V, Bauer RW. High-pitch dual-source CT angiography of the whole aorta without ECG synchronisation: initial experience. Eur Radiol. 2012;22(1):129–37.
27. Wuest W, Anders K, Schuhbaeck A, May MS, Gauss S, Marwan M, Arnold M, Ensminger S, Muschiol G, Daniel WG, Uder M, Achenbach S. Dual source multidetector CT-angiography before Transcatheter Aortic Valve Implantation (TAVI) using a high-pitch spiral acquisition mode. Eur Radiol. 2012;22(1):51–8.
28. Plank F, Friedrich G, Bartel T, Mueller S, Bonaros N, Heinz A, Klauser A, Cartes-Zumelzu F, Grimm M, Feuchtner G. Benefits of high-pitch 128-slice dual-source computed tomography for planning of transcatheter aortic valve implantation. Ann Thorac Surg. 2012;94(6):1961–6.
29. Hsiao EM, Rybicki FJ, Steigner M. CT coronary angiography: 256-slice and 320-detector row scanners. Curr Cardiol Rep. 2010;12(1):68–75. https://doi.org/10.1007/s11886-009-0075-z.
30. Ohno Y, Koyama H, Matsumoto K, Onishi Y, Takenaka D, Fujisawa Y, Yoshikawa T, Konishi M, Maniwa Y, Nishimura Y, Ito T, Sugimura K. Differentiation of malignant and benign pulmonary nodules with quantitative first-pass 320-detector row perfusion CT versus FDG PET/CT. Radiology. 2011;258(2):599–609.
31. Willems PW, Taeshineetanakul P, Schenk B, Brouwer PA, Terbrugge KG, Krings T. The use of 4D-CTA in the diagnostic work-up of brain arteriovenous malformations. Neuroradiology. 2012;54(2):123–31.
32. Motosugi U, Ichikawa T, Sou H, Morisaka H, Sano K, Araki T. Multi-organ perfusion CT in the abdomen using a 320-detector row CT scanner: preliminary results of perfusion changes in the liver, spleen, and pancreas of cirrhotic patients. Eur J Radiol. 2012;81(10):2533–7.
33. US Patent X-Ray transmission scanning system and method and electron beam X-ray scan tube for use therewith. US 4352021. 1982.
34. Agatston AS, Janowitz WR, Hildner FJ, et al. Quantification of coronary artery calcium using ultrafast computed tomography. J Am Coll Cardiol. 1990;15(4):827–32.
35. Achenbach S, Ropers D, Regenfus M, Muschiol G, Daniel WG, Moshage W. Contrast enhanced electron beam computed tomography to analyse the coronary arteries in patients after acute myocardial infarction. Heart. 2000;84(5):489–93.
36. Rumberger JA, Sheedy PF, Breen JF. Use of ultrafast (cine) x-ray computed tomography in cardiac and cardiovascular imaging. In: Giuliani ER, Gersh BJ, McGoon MD, Hayes DL, Schaff HF, editors. Mayo clinic practice of cardiology. 3rd ed. St. Louis: Mosby; 1996. p. 303–24.
37. Bell MR, Lerman LO, Rumberger JA. Validation of minimally invasive measurement of myocardial perfusion using electron beam computed tomography and application in human volunteers. Heart. 1999;81:628–35.
38. Lu B, Zhuang N, Mao S, Bakhsheshhi H, Liu S, Budoff M. Image quality of three-dimensional electron beam coronary angiography. J Comput Assist Tomogr. 2002;26:202–9.
39. Niemann T, Henry S, Duhamel A, Faivre JB, Deschildre A, Colas L, Santangelo T, Remy J, Remy-Jardin M. Pediatric chest CT at 70 kVp: a feasibility study in 129 children. Pediatr Radiol. 2014;44(11):1347–57.
40. Durand S, Paul JF. Comparison of image quality between 70 kVp and 80 kVp: application to paediatric cardiac CT. Eur Radiol. 2014;24(12):3003–9.
41. LaBounty TM, Leipsic J, Poulter R, et al. Coronary CT angiography of patients with a normal body mass index using 80 kVp versus 100 kVp: a prospective, multicenter, multivendor randomized trial. AJR Am J Roentgenol. 2011;197(5):W860–7.
42. Oda S, Utsunomiya D, Funama Y, et al. A low tube voltage technique reduces the radiation dose at retrospective ECG-gated cardiac computed tomography for anatomical and functional analyses. Acad Radiol. 2011;18(8):991–9.
43. Nakagawa M, Ozawa Y, Sakurai K, Shimohira M, Ohashi K, Asano M, Yamaguchi S, Shibamoto Y. Image quality at low tube voltage (70 kV) and sinogram-affirmed iterative reconstruction for computed tomography in infants with congenital heart disease. Pediatr Radiol. 2015;45(10):1472–9.
44. Duan X, Wang J, Leng S, Schmidt B, Allmendinger T, Grant K, Flohr T, McCollough CH. Electronic noise in CT detectors: impact on image noise and artifacts. AJR Am J Roentgenol. 2013;201(4):W626–32.
45. Flohr T, Stierstorfer K, Raupach R, Ulzheimer S, Bruder H. Performance evaluation of a 64-slice CT-system with z-flying focal spot. Rofo. 2004;176:1803–10.
46. Flohr TG, Stierstorfer K, Ulzheimer S, Bruder H, Primak AN, McCollough CH. Image reconstruction and image quality

evaluation for a 64-slice CT scanner with z-flying focal spot. Med Phys. 2005;32(8):2536–47.
47. Lee AM, Beaudoin J, Engel LC, Sidhu MS, Abbara S, Brady TJ, Hoffmann U, Ghoshhajra BB. Assessment of image quality and radiation dose of prospectively ECG-triggered adaptive dual-source coronary computed tomography angiography (cCTA) with arrhythmia rejection algorithm in systole versus diastole: a retrospective cohort study. Int J Cardiovasc Imaging. 2013;29(6):1361–70.
48. Flohr TG, Schoepf UJ, Ohnesorge BM. Chasing the heart: new developments for cardiac CT. J Thorac Imaging. 2007;22(1):4–16.
49. Muenzel D, Noel PB, Dorn F, Dobritz M, Rummeny EJ, Huber A. Coronary CT angiography in step-and-shoot technique with 256-slice CT: impact of the field of view on image quality, craniocaudal coverage, and radiation exposure. Eur J Radiol. 2012;81(7):1562–8.
50. Klass O, Walker M, Siebach A, Stuber T, Feuerlein S, Juchems M, Hoffmann MH. Prospectively gated axial CT coronary angiography: comparison of image quality and effective radiation dose between 64- and 256-slice CT. Eur Radiol. 2010;20(5):1124–31.
51. Rybicki FJ, Otero HJ, Steigner ML, Vorobiof G, Nallamshetty L, Mitsouras D, Ersoy H, Mather RT, Judy PF, Cai T, Coyner K, Schultz K, Whitmore AG, Di Carli MF. Initial evaluation of coronary images from 320-detector row computed tomography. Int J Cardiovasc Imaging. 2008;24(5):535–46.
52. Tomizawa N, Maeda E, Akahane M, Torigoe R, Kiryu S, Ohtomo K. Coronary CT angiography using the second-generation 320-detector row CT: assessment of image quality and radiation dose in various heart rates compared with the first-generation scanner. Int J Cardiovasc Imaging. 2013;29(7):1613–8.
53. Engel KJ, Herrmann C, Zeitler G. X-ray scattering in single- and dual-source CT. Med Phys. 2008;35(1):318–32.
54. Vogtmeier G, Dorscheida R, Engela KR, Luhtab K, Mattsonb R, Harwoodb B, Applebyc M, Randolphc B, KlingerVogtmeier J, et al. Two-dimensional anti-scatter grids for computed tomography detectors. Medical imaging. International Society for Optics and Photonics. 2008.
55. Li B, Toth TL, Hsieh J, et al. Simulation and analysis of image quality impacts from single source, ultra-wide coverage CT scanner. J Xray Sci Technol. 2012;20(4):395–404.
56. Chen MY, Shanbhag SM, Arai AE. Submillisievert median radiation dose for coronary angiography with a second-generation 320-detector row CT scanner in 107 consecutive patients. Radiology. 2013;267(1):76–85.
57. Nasis A, Leung MC, Antonis PR, Cameron JD, Lehman SJ, Hope SA, Crossett MP, Troupis JM, Meredith IT, Seneviratne SK. Diagnostic accuracy of noninvasive coronary angiography with 320-detector row computed tomography. Am J Cardiol. 2010;106(10):1429–35.
58. Kondo T, Kumamaru KK, Fujimoto S, Matsutani H, Sano T, Takase S, Rybicki FJ. Prospective ECG-gated coronary 320-MDCT angiography with absolute acquisition delay strategy for patients with persistent atrial fibrillation. AJR Am J Roentgenol. 2013;201(6):1197–203.
59. George RT, Mehra VC, Chen MY, Kitagawa K, Arbab-Zadeh A, Miller JM, Matheson MB, Vavere AL, Kofoed KF, Rochitte CE, Dewey M, Yaw TS, Niinuma H, Brenner W, Cox C, Clouse ME, Lima JA, Di Carli M. Myocardial CT perfusion imaging and SPECT for the diagnosis of coronary artery disease: a head-to-head comparison from the CORE320 multicenter diagnostic performance study. Radiology. 2015;274(2):626.
60. Sharma RK, Arbab-Zadeh A, Kishi S, Chen MY, Magalhães TA, George RT, Dewey M, Rybicki FJ, Kofoed KF, de Roos A, Tan SY, Matheson M, Vavere A, Cox C, Clouse ME, Miller JM, Brinker JA, Arai AE, Di Carli MF, Rochitte CE, Lima JA. Incremental diagnostic accuracy of computed tomography myocardial perfusion imaging over coronary angiography stratified by pre-test probability of coronary artery disease and severity of coronary artery calcification: the CORE320 study. Int J Cardiol. 2015;201:570–7.
61. So A, Imai Y, Nett B, Jackson J, Nett L, Hsieh J, Wisenberg G, Teefy P, Yadegari A, Islam A, Lee TY. Technical Note: Evaluation of a 160-mm/256-row CT scanner for whole-heart quantitative myocardial perfusion imaging. Med Phys. 2016;43(8):4821. https://doi.org/10.1118/1.4957389.
62. FDA, 510k Summary Document https://www.accessdata.fda.gov/cdrh_docs/pdf16/K161066.pdf
63. Sun ML, Lu B, Wu RZ, Johnson L, Han L, Liu G, Yu FF, Hou ZH, Gao Y, Wang HY, Jiang S, Yang YJ, Qiao SB. Diagnostic accuracy of dual-source CT coronary angiography with prospective ECG-triggering on different heart rate patients. Eur Radiol. 2011;21(8):1635–42.
64. Lee AM, Engel LC, Shah B, Liew G, Sidhu MS, Kalra M, Abbara S, Brady TJ, Hoffmann U, Ghoshhajra BB. Coronary computed tomography angiography during arrhythmia: radiation dose reduction with prospectively ECG-triggered axial and retrospectively ECG-gated helical 128-slice dual-source CT. J Cardiovasc Comput Tomogr. 2012;6(3):172–183.e2.
65. Paul JF, Amato A, Rohnean A. Low-dose coronary-CT angiography using step and shoot at any heart rate: comparison of image quality at systole for high heart rate and diastole for low heart rate with a 128-slice dual-source machine. Int J Cardiovasc Imaging. 2013;29(3):651–7.
66. Westwood ME, Raatz HD, Misso K, Burgers L, Redekop K, Lhachimi SK, Armstrong N, Kleijnen J. Systematic review of the accuracy of dual-source cardiac CT for detection of arterial stenosis in difficult to image patient groups. Radiology. 2013;267(2):387–95.
67. Sidhu MS, Venkatesh V, Hoffmann U, et al. Advanced adaptive axial-sequential prospectively electrocardiogram-triggered dual-source coronary computed tomographic angiography in a patient with atrial fibrillation. J Comput Assist Tomogr. 2011;35(6):747–8.
68. Hutt A, Tacelli N, Faivre JB, Flohr T, Duhamel A, Remy J, Remy-Jardin M. Is bronchial wall imaging affected by temporal resolution? Comparative evaluation at 140 and 75 ms in 90 patients. Eur Radiol. 2016;26(2):469–77.
69. Petersilka M, Stierstorfer K, Bruder H, Flohr T. Strategies for scatter correction in dual source CT. Med Phys. 2010;37(11):5971–92.
70. T G F, Leng S, Yu L, Allmendinger T, Bruder H, Petersilka M, Eusemann CD, Stierstorfer K, Schmidt B, McCollough C. Dual-source spiral CT with pitch up to 3.2 and 75 ms temporal resolution: image reconstruction and assessment of image quality. Med Phys. 2009;36(12):5641–53.
71. Hou DJ, Tso DK, Davison C, Inacio J, Louis LJ, Nicolaou S, Reimann AJ, Hou DJ, Tso DK, Davison C, Inacio J, Louis LJ, Nicolaou S, Reimann AJ. Clinical utility of ultra high pitch dual source thoracic CT imaging of acute pulmonary embolism in the emergency department: are we one step closer towards a non-gated triple rule out? Eur J Radiol. 2013;82(10):1793–8.
72. Apfaltrer P, Hanna EL, Schoepf UJ, Spears JR, Schoenberg SO, Fink C, Vliegenthart R. Radiation dose and image quality at high-pitch CT angiography of the aorta: intraindividual and interindividual comparisons with conventional CT angiography. AJR Am J Roentgenol. 2012;199(6):1402–9.
73. Han BK, Overman DM, Grant K, et al. Non-sedated, free breathing cardiac CT for evaluation of complex congenital heart disease in neonates. J Cardiovasc Comput Tomogr. 2013;7(6):354–60.
74. Lee JH, Han D, Danad I, et al. Multimodality imaging in coronary artery disease: focus on computed tomography. J Cardiovasc Ultrasound. 2016;24(1):7–17.
75. Lell MM, May M, Deak P, Alibek S, Kuefner M, Kuettner A, Köhler H, Achenbach S, Uder M, Radkow T. High-pitch spiral computed tomography: effect on image quality and radiation dose in pediatric chest computed tomography. Investig Radiol. 2011;46(2):116–23.

76. Bridoux A, Hutt A, Faivre JB, Flohr T, Duhamel A, Pagniez J, Remy J, Remy-Jardin M. Coronary artery visibility in free-breathing young children on non-gated chest CT: impact of temporal resolution. Pediatr Radiol. 2015;45(12):1761–70.
77. Achenbach S, Marwan M, Schepis T, Pflederer T, Bruder H, Allmendinger T, Petersilka M, Anders K, Lell M, Kuettner A, Ropers D, Daniel WG, Flohr T. High-pitch spiral acquisition: a new scan mode for coronary CT angiography. J Cardiovasc Comput Tomogr. 2009;3:117–21.
78. Leschka S, Stolzmann P, Desbiolles L, Baumueller S, Goetti R, Schertler T, Scheffel H, Plass A, Falk V, Feuchtner G, Marincek B, Alkadhi H. Diagnostic accuracy of high-pitch dual-source CT for the assessment of coronary stenoses: first experience. Eur Radiol. 2009;19(12):2896–903.
79. Gordic S, Husarik DB, Desbiolles L, Leschka S, Frauenfelder T, Alkadhi H. High-pitch coronary CT angiography with third generation dual-source CT: limits of heart rate. Int J Cardiovasc Imaging. 2014;30(6):1173–9.
80. Morsbach F, Gordic S, Desbiolles L, Husarik D, Frauenfelder T, Schmidt B, Allmendinger T, Wildermuth S, Alkadhi H, Leschka S. Performance of turbo high-pitch dual-source CT for coronary CT angiography: first ex vivo and patient experience. Eur Radiol. 2014;24(8):1889–95.
81. Azzalini L, Abbara S, Ghoshhajra BB. Ultra-low contrast computed tomographic angiography (CTA) with 20-mL total dose for transcatheter aortic valve implantation (TAVI) planning. J Comput Assist Tomogr. 2014;38(1):105–9.